Research Article Vol. 3, No. 3 / 15 March 2020 / OSA Continuum 580
OSA CONTINUUM

Alignment tolerant dual-surface sphero-cylindrical progressive addition lens

YIYU LI,[1,2,*] XIAOLI HU,[1,2] HUILV JIANG,[1,2] HAIHUA FENG,[1,2] AND HAO CHEN[1,2]

[1] School of Optometry and Ophthalmology, WenZhou Medical University, ZheJiang, 325000, China
[2] The Affiliated Eye Hospital of WenZhou Medical University, ZheJiang, 325000, China
[*] liyiyu@wmu.edu.cn

Abstract: We present the design, fabrication, and characterization of a dual-surface sphero-cylindrical progressive addition lens (DSOC-PAL), which combines the progressive cylindrical addition power of both lens surfaces to give the required spherical addition power. Both the freeform lens surfaces are numerically solved with the variational-difference numerical method based on the minimization of a merit function that employs weight functions and boundary conditions to balance between the desired spherical power distribution and the necessary cylindrical power distribution. The simulation results show that the proposed DSOC-PAL design is highly tolerant to the surface alignment errors and agree well with the experimental results obtained by the lens surfacing and polishing process.

1. Introduction

The progressive power lens is widely used for presbyopia because it enables clear visual refocusing across a continuous range of distances [1]. With two lens surfaces to work with, the conventional anterior progressive lenses represent a combination of factory-molded progressive surface on the front and freeform surfaced prescription curves on the back. The posterior progressive lenses employ a factory-molded spherical surface on the front and a freeform progressive surface with prescription curves on the back. Besides, the dual-surface progressive lenses allot a portion of spherical addition power (SAP) on the front surface with base curve and the remaining addition power on the back surface with prescription curves that has been optically optimized. Regardless of the placement of the actual SAP, the magnitude of the unwanted astigmatism and the skew distortion may not be significantly influenced, because the surface powers of each surface are essentially additive by using thin lens approximation for the lens of fairly negligible thickness.

In order to improve the distortion and minimize the sway of an image caused by the magnification difference between a distance portion and a near portion of progressive lens, the SAP is decomposed into two axially orthogonal cylindrical addition powers (CAP) which are separately located on each surface of lens [2,3]. In general, the anterior surface features a combination of base curves and progressive cylindrical optics oriented at vertical axis, while the posterior surface features a combination of prescription curves and progressive cylindrical optics oriented at horizontal axis. This dual-surface sphero-cylindrical progressive addition lens (DSOC-PAL) has an advantage of increasing the visual field in the horizontal direction with less skew distortion in wearing.

The early design models of progressive lenses employed the surface geometry represented by horizontal conic sections that gradually increase in curvature down the progressive region, resulting in a rapid increase in mean power and irregular surface astigmatism or unwanted cylindrical power [4]. Later, the use of smoothing functions in the direct design method [5,6] reduced the surface astigmatism in the peripheral lens region, while providing an easy way to adjust the area of viewing zone. However, the peak level of the remaining surface astigmatism

#385544 https://doi.org/10.1364/OSAC.385544
Journal © 2020 Received 11 Dec 2019; revised 27 Feb 2020; accepted 2 Mar 2020; published 6 Mar 2020

OSA CONTINUUM

still exceeded the magnitude of the addition power and concentrated in the lateral small regions close to the progressive corridor, resulting in a narrow intermediate zone of variable focus.

Recently, progressive lens design was simplified as a functional minimization problem in several indirect methods [7,8] that construct a merit function to match the desired distribution of spherical power with the minimized unwanted surface astigmatism, no matter whether the SAP is placed on the anterior surface, posterior surface or allotted between two surfaces. Numerical methods such as B-spline finite element method [9] and variational-difference method [10] have been proposed to minimize the merit function efficiently. With the addition of spectacle frame function, the indirect methods have been successfully used to design customized progressive lenses of the lowest level of surface astigmatism [11]. However, in the case of DSOC-PAL design, because of the required distribution of necessary CAP on both surfaces, the existing indirect methods that aim to eliminate the unwanted cylindrical power is believed to be unsuitable to solve this sphero-cylindrical progressive surfaces.

In this paper, we extend the capability of the indirect method to cover the DSOC-PAL design, and show that the desired distribution of both CAP and spherical power can be realized simultaneously by carefully constructing the weight functions and the boundary conditions for a merit function which can be minimized by using the variational-difference numerical method. Additionally, the influence of the surface misalignments on lens powers are simulated to predict the alignment tolerance for the lens surfacing process. Subsequently, we use computer-controlled three-axis freeform generator to fabricate the complex lens surfaces by a diamond turning process assisted by fast tool servo (FTS).

2. Surface design and representation

2.1. Configuration of merit function

In the case of conventional progressive lens with SAP, for the purpose to match the desired distribution of spherical power with the minimal distribution of surface astigmatism, the indirect method of lens design formulates the surface optimization problem as the minimization of the following merit function:

$$\mathrm{MF} = \int_{\Omega} \left\{ \alpha(x,y) \left[\frac{\kappa_1(x,y) - \kappa_2(x,y)}{2} \right]^2 + \beta(x,y)[H(x,y) - H_r(x,y)]^2 \right\} dxdy \tag{1}$$

where $\kappa_1(x, y)$ and $\kappa_2(x, y)$ are the principal curvatures that can be used to define the mean curvature $H(x, y)$ as:

$$H(x,y) = \frac{\kappa_1(x,y) + \kappa_2(x,y)}{2} \tag{2}$$

$H_r(x, y)$ represents the desired distribution of mean curvature. The difference between the two principal curvatures is related to the surface astigmatism by using

$$A(x,y) = (\mathrm{RI} - 1)|\kappa_1(x,y) - \kappa_2(x,y)| \tag{3}$$

where RI is the refractive index of lens material. Thereby, $\alpha(x, y)$ and $\beta(x, y)$ are two positive weight functions for surface astigmatism and mean curvature, respectively. Strong weighting factor should be assigned both for $\alpha(x, y)$ and $\beta(x, y)$ in the area of clear vision zone for conventional progressive lens design.

Assuming that the progressive surfaces are a combination of a spherical background surface and a perturbation surface, the minimization of merit function can be linearized and simplified to a quadratic functional minimization problem which can be numerically solved. This method has been well performed in reducing the peak level of surface astigmatism that could be lower than the magnitude of addition power both for anterior progressive lenses design [10] and posterior

OSA CONTINUUM

progressive lenses design [11]. However, in the case of DSOC-PAL, the weight functions used in merit function must be reconfigured, otherwise the desired distribution of CAP will be considered as unwanted surface astigmatism and minimized by mistake.

The initial design parameters of DSOC-PAL are based on the patient's prescription, for example, an emmetropic patient suffering from presbyopia of 2.00 diopter. Lens can be designed with a combination of a front base curve of 4.00 diopter with CAP of 2.00 diopter oriented at vertical axis and a back prescription curve of -4.00 diopter with CAP of 2.00 diopter oriented at horizontal axis. For all the following simulations, we choose the refractive index of 1.60 and lens central thickness of 3.5 mm. The distance from the distance reference point (DRP) to the lens geometrical center along the vertical meridian is 7 mm. The progressive corridor length from the geometrical center to the near reference point (NRP) is set to be 12 mm.

2.2. Anterior surface of sphero-cylindrical progressive design

In the distance zone, the anterior lens surface is approximately spherical with curvature of 6.67 m^{-1}. From DRP to NRP, the surface should provide a progressive increase in vertical curvature through the vertical meridian while the curvature of the horizontal cross-section keeps constant. Therefore, a progressive CAP oriented at vertical axis can be established, and the near zone features a stable sphero-cylindrical surface. The principal curvatures at NRP is calculated to be $\kappa_1 = 6.67$ m^{-1} at horizontal direction and $\kappa_2 = 10$ m^{-1} at vertical direction, respectively.

To design such an anterior lens surface, a relatively large weighting factor is assigned in the distance zone of $y > 10$ mm for $\alpha(x, y)$ as shown in Fig. 1(a). The weighting factor should decrease in value from DRP to NRP, then keep a minimal value in the near zone of $y < -15$ mm so that the required cylindrical power can be maintained in this area. For weight function $\beta(x, y)$, a uniform distribution of weighting factor is assigned across the whole surface. The mean curvature $H_r(x, y)$ features a uniform distribution both in the distance zone and the near zone, while all the vertical cross-sections duplicate the distribution of mean curvature through the vertical meridian.

A spherical background surface with radius of curvature $R = 151$ mm is chosen to solve the minimization problem of the merit function. Additional boundary conditions that guarantee the same sag value at both ends of the horizontal cross-sections are employed in the numerical optimization of the perturbation surface of the anterior surface as shown in Fig. 1.

2.3. Posterior surface of sphero-cylindrical progressive design

In the distance zone, the posterior lens surface is approximately spherical with curvature of 6.73 m^{-1}. From DRP to NRP, the surface should provide a progressive decrease in horizontal curvature while the vertical curvature through the vertical meridian keeps constant. Therefore, the distribution of progressive CAP oriented at horizontal axis can be established. Meanwhile, the sphero-cylindrical power should remain stable in the near zone, so that it can be coupled with the crossed sphero-cylindrical powers of the opposite surface at corresponding points to give the desired SAP. The principal curvatures at NRP is calculated to be $\kappa_1 = 3.31$ m^{-1} at horizontal direction and $\kappa_2 = 6.73$ m^{-1} at vertical direction.

To design such a posterior lens surface, a large weighting factor is assigned in the distance zone for $\alpha(x, y)$ as shown in Fig. 2(a). The area of distance zone has shrunk compared with that of the opposite surface. The remaining region of $\alpha(x, y)$ is uniformly assigned a slight weighting factor. For weight function $\beta(x, y)$, only the central region along the vertical meridian is highly weighted, while the remaining region is slightly weighted to enable a free distribution of mean curvature. Unlike the case of anterior surface, here the lower portion of the highly weighted region in $\beta(x, y)$ defines the near zone on the posterior surface. This near zone has been linearly shifted by 2 mm to the nasal side as the lens design is performed for the right eye. From DRP to NRP, the mean curvature $H_r(x, y)$ decreases in value along the vertical median. Then, for the

OSA CONTINUUM

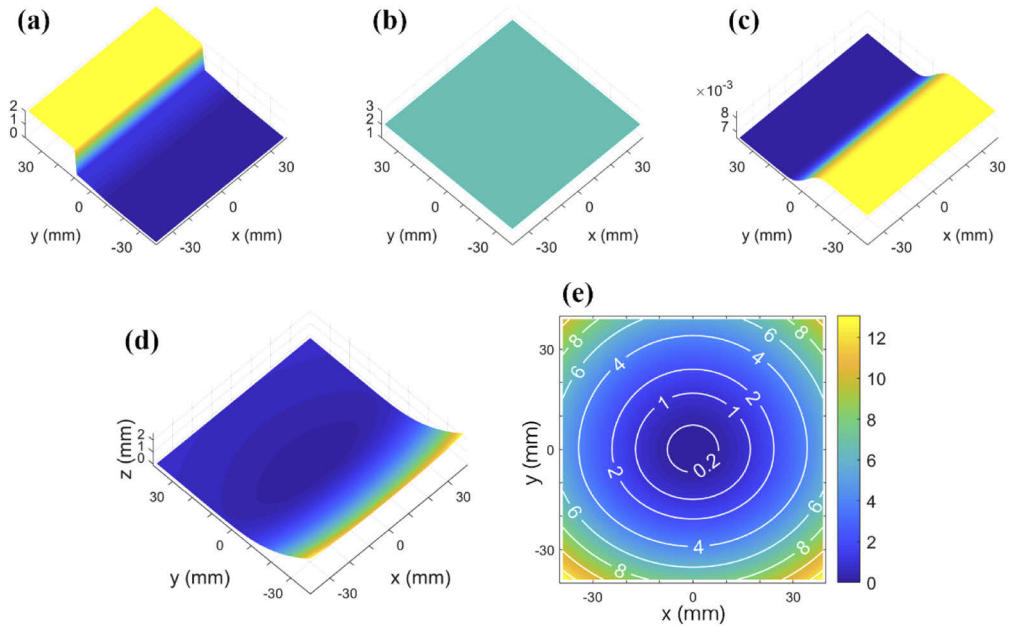

Fig. 1. The (a) weight function $\alpha(x, y)$, (b) weight function $\beta(x, y)$ and (c) mean curvature $H_r(x,y)$ are required in the merit function for the anterior lens surface design. The numerically solved (d) perturbation surface is combined with a spherical background surface with radius of curvature $R = 151$ mm to give (e) the anterior surface of DSOC-PAL.

other points on the posterior surface, the mean curvatures are determined according to the ratio of their distances to DRP and NRP.

The numerical optimization procedure is almost the same as that of the anterior surface. The difference is that the spherical background surface with radius of curvature $R = 149.4$ mm is chosen for the posterior surface. Meanwhile, the boundary conditions are updated to guarantee the same sag value along the vertical meridian of perturbation surface as shown in Fig. 2(e).

2.4. *Surface representation and lens power calculation*

In ophthalmic optics, the cloud points of surface are usually fit by Zernike circle polynomials [12] due to their property of orthogonality over a unit circular domain which matches with the shape of lenses or pupils. The examples can be found in the fitting of wavefront surfaces [13,14] and corneal surfaces [15,16]. Previous study has proved that a RMS fitting error of less than 30 nm can be achieved with Zernike polynomials by using the standard least squares fitting method for the freeform surface of progressive lens [17,18].

Here, in order to represent the surfaces of DSOC-PAL, Zernike polynomials up to 16th order are employed in surface fitting with sampling subgrid size of 1.0 mm × 1.0 mm. Zernike polynomial coefficients, as shown in Fig. 3, are calculated over a lens aperture of 78 mm in diameter. Major difference between the two surfaces can be found in mode 5 (named vertical astigmatism) and mode 7 (named vertical coma) due to the orthogonal axes of progressive CAP.

Following the definition of dioptric power, lens surface powers can be the product of normal curvatures that change continuously on the freeform surfaces and the difference of refractive index between lens material and air. The differential geometry theorem [19] states that the normal curvature of an arbitrary normal section can be expressed in terms of the principal curvatures that measure the maximum and minimum bending at the given point on a surface. Therefore, the

OSA CONTINUUM

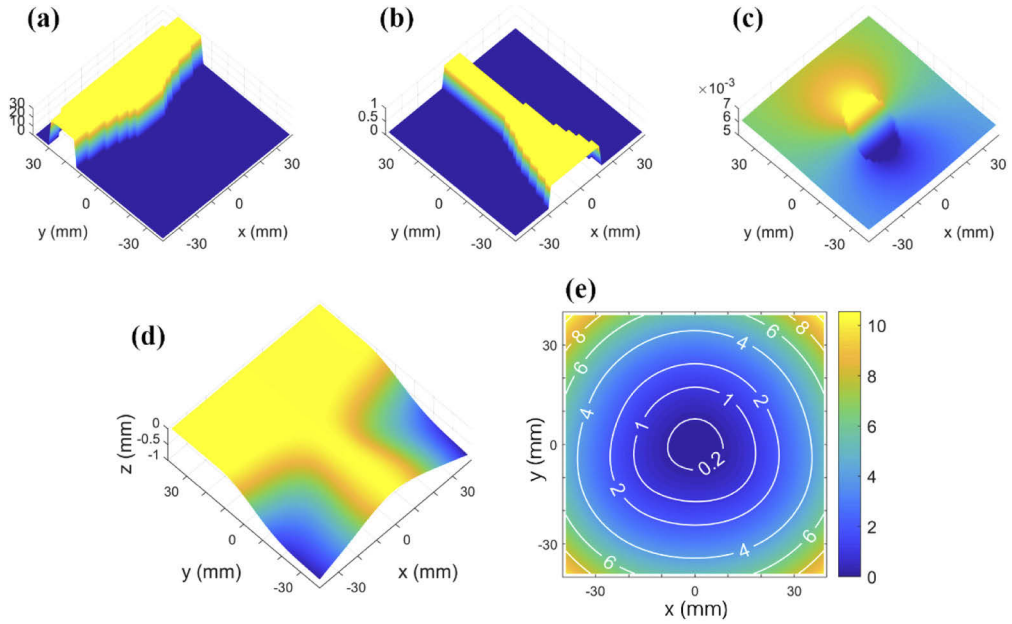

Fig. 2. The (a) weight function $\alpha(x, y)$, (b) weight function $\beta(x, y)$ and (c) mean curvature $H_r(x,y)$ are required in the merit function for the posterior lens surface design. The numerically solved (d) perturbation surface is combined with a spherical background surface with radius of curvature $R = 149.4$ mm to give (e) the posterior surface of DSOC-PAL.

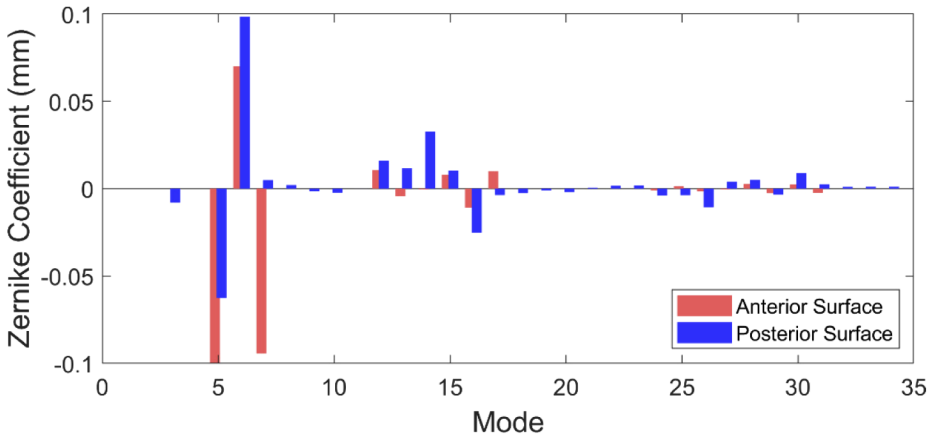

Fig. 3. Zernike coefficients of lens surfaces except mode 4 and the modes less than 3.

principal curvatures can give the maximum and minimum surface power, usually called high power P_h and low power P_l, respectively at that point on surface in lens industry.

The principal curvatures κ_1 and κ_2 of the lens surface $S(x, y)$ are the roots of the following fundamental quadratic equation:

$$(EG - F^2)\kappa^2 - (EN + GL - 2FM)\kappa + (LN - M^2) = 0 \tag{4}$$

$$E = 1 + S_x^2, \quad F = S_x S_y, \quad G = 1 + S_y^2,$$

OSA CONTINUUM

$$L = \frac{S_{xx}}{\sqrt{1 + S_x^2 + S_y^2}}, \quad M = \frac{S_{xy}}{\sqrt{1 + S_x^2 + S_y^2}}, \quad N = \frac{S_{yy}}{\sqrt{1 + S_x^2 + S_y^2}}$$

Since Zernike polynomials have been expressed in terms of powers of x and y at Cartesian coordinate system for the representation of lens surface, the first-order derivatives S_x and S_y and the second-order derivatives S_{xx}, S_{xy} and S_{yy} which are continuous everywhere on the surface can be calculated algebraically.

The calculated distributions of high power and surface astigmatism have been shown in Fig. 4 for both surfaces. In the case of DSOC-PAL design, the surface astigmatism is also referred to as local cylindrical power. According to Eq. (3), local cylindrical power is actually defined as the difference between high power and low power at each point on the surfaces. The arrows displayed with cylindrical powers indicate the principal directions of high powers and are also considered as the axial orientation of cylindrical power. As we expected, the anterior surface possesses a distribution of progressive CAP oriented at vertical axis. In the case of posterior surface, only in the limited near zone close to the vertical meridian is there regular distribution of progressive CAP oriented at horizontal axis.

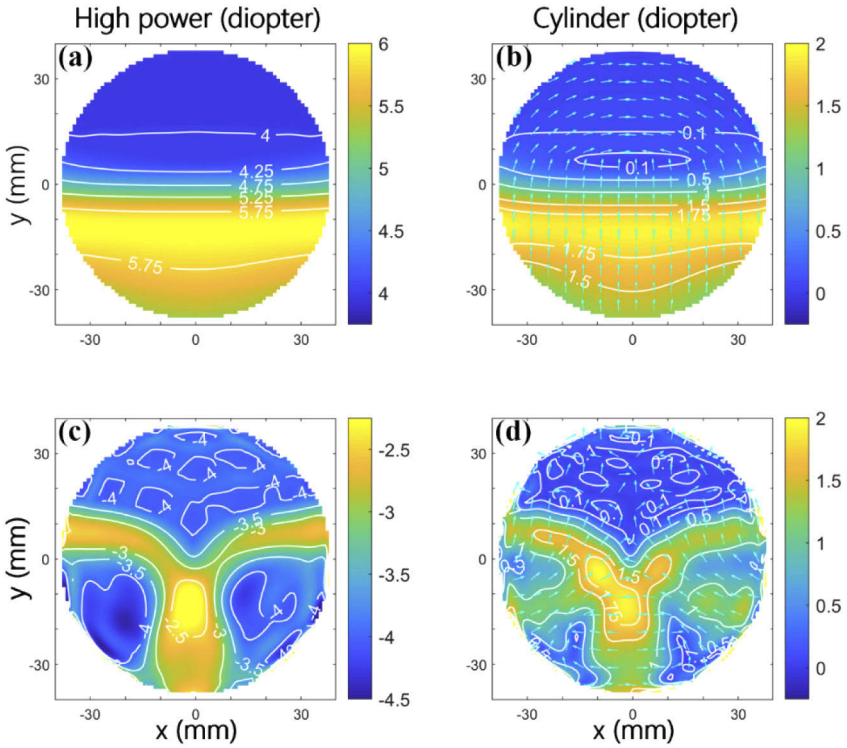

Fig. 4. The simulated surface power distribution of DSOC-PAL. (a) High power and (b) cylindrical power of the anterior lens surface; (c) high power and (d) cylindrical power of the posterior lens surface.

Lens power is the combined contribution of both lens surfaces. However, due to the discrepancy in the orientation of cylindrical power at each point between the two surfaces, the surface power distributions shown in Fig. 4 cannot be added directly. In order to obtain the lens power distribution, the surface powers should be converted to power vectors [20] as shown in Fig. 5(a)–5(f) by using

OSA CONTINUUM

the following equations:

$$M(x,y) = \frac{P_h(x,y) + P_l(x,y)}{2}$$
$$J_0(x,y) = -\frac{A(x,y)}{2}\cos 2\varphi(x,y) \tag{5}$$
$$J_{45}(x,y) = -\frac{A(x,y)}{2}\sin 2\varphi(x,y)$$

where $M(x, y)$ is equivalent spherical power, $J_0(x, y)$ is cylinder component at 0-degree meridian, $J_{45}(x, y)$ is cylinder component at 45-degree meridian, and $\varphi(x, y)$ is principal direction of high power. A matrix of power vector [M, J_0, J_{45}] can be constructed for each lens surface.

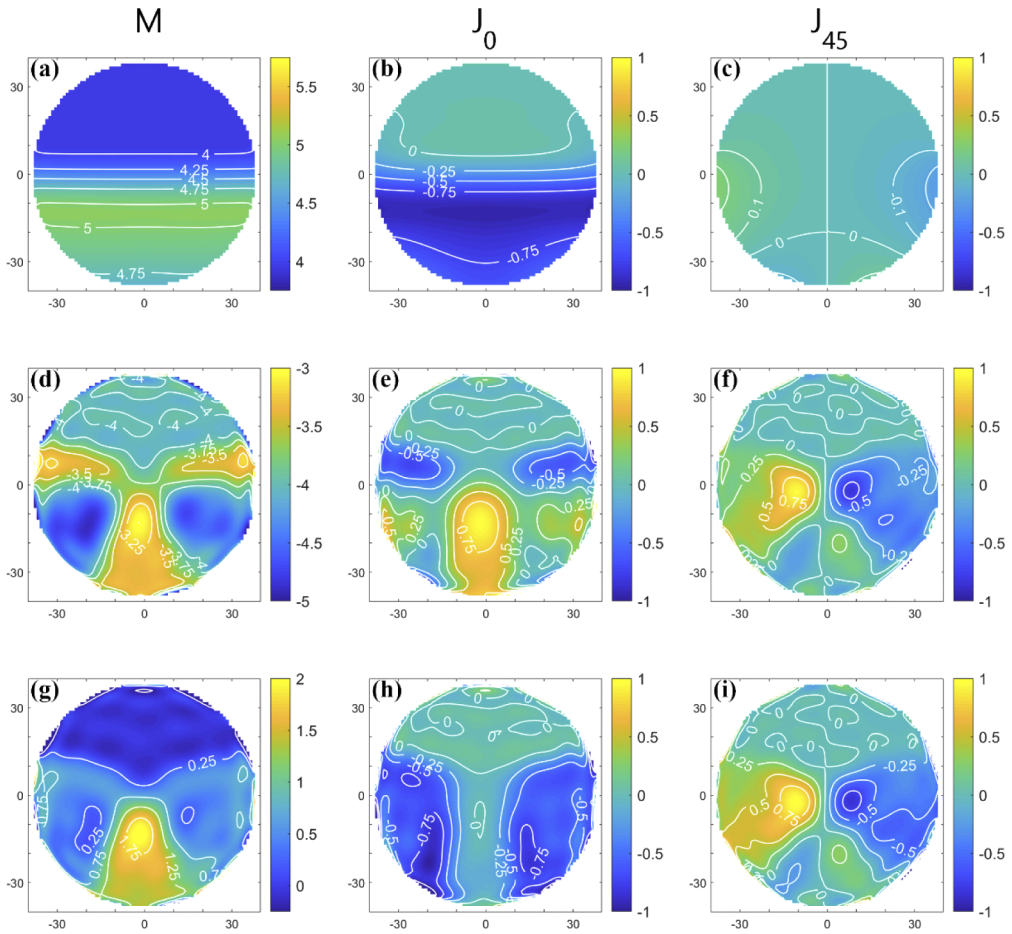

Fig. 5. The power vector representation of the designed DSOC-PAL. (a)~(c) The anterior lens surface and (d)~(f) the posterior lens surface are combined to give (g)~(i) the whole lens.

By considering thin lens approximation, adding the corresponding elements of the two matrices results in power vector representation [M_{a+p}, $J_{0,a+p}$, $J_{45,a+p}$] of the whole lens as shown in Fig. 5(g)–5(i). By using the following equations, the power vectors can be converted back to the conventional sphero-cylinder representation of lens powers as shown in Fig. 6 which can be

OSA CONTINUUM

understood by the optometrists.

$$Cyl = 2\sqrt{J^2_{0,\,a+p} + J^2_{45,\,a+p}}$$
$$High\ Power = M_{a+p} + \frac{Cyl}{2} \tag{6}$$

The sphero-cylinder maps illustrated in Fig. 6 demonstrate that the change in cylindrical power lateral to the corridor is roughly equal to twice the change in SAP along the corridor, which is the nature of progressive optics as explained by Minkwitz's theorem [21,22] that has rules the design of conventional anterior progressive lenses and posterior progressive lenses.

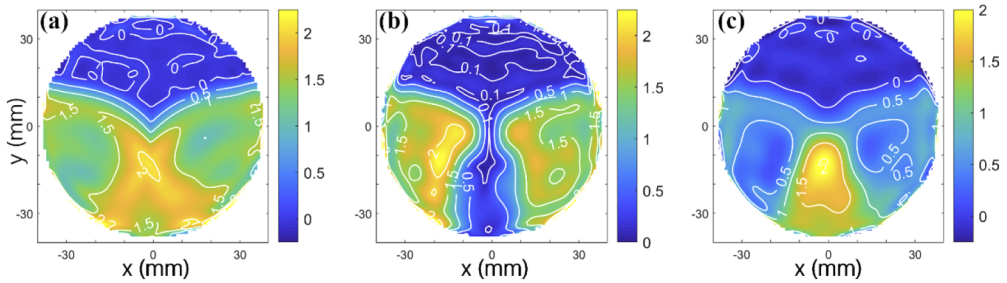

Fig. 6. The sphero-cylinder representation of the surface power of DSOC-PAL, including (a) high power, (b) cylindrical power and (c) equivalent spherical power that is actually the same as Fig. 5(g).

The surface power maps can hardly give an accurate picture of the lens performance when worn. So, a ray tracing of the lens was performed for each gaze direction to calculate the optical power distribution at the vertex sphere interface which has a radius curvature of 25 mm with a curvature center representing the eyeball rotation center. The fitting point on the lens is set at the middle point between the DRP and the lens geometrical center. The eyeball rotation center is aligned with the fitting point to represent the gaze direction of zero degree. As shown in Fig. 7, the actual distance zone perceived by the wearer is slightly reduced, while the near zone is relatively enlarged, because a typical pantoscopic (vertical) tilt of 7 degree and a face-form (horizontal) wrap of 5 degree were employed to position the lens in fitting geometry for the ray tracing. Extreme low level of astigmatism with the value of 0.03 diopter is obtained when gazing through the DRP or NRP on the lens.

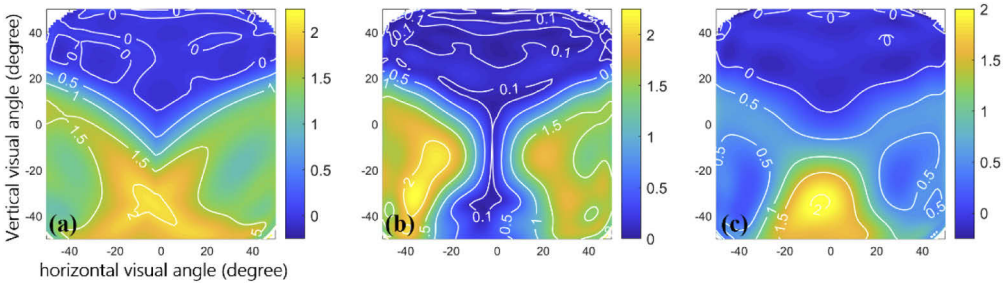

Fig. 7. The optical performance including (a) high power, (b) astigmatism and (c) equivalent spherical power in diopters calculated by ray tracing of the designed DSOC-PAL at each gaze direction.

OSA CONTINUUM

3. Surface misalignment and lens power deviation

The two surfaces of DSOC-PAL are produced by freeform generators in sequential order, so it is important to ensure the surface alignment accuracy. Otherwise, the surface misalignment may cause lens power deviation, thereby deteriorating the lens wearing performance. The major source of surface misalignment is the lens blocking process which connects a lens blank or a semi-finished lens blank and a positioning unit with low temperature alloy. Before the machining of anterior lens surface, the posterior surface of a lens blank should be blocked first. After finishing of the anterior surface, this semi-finished lens blank should be deblocked and then re-blocked on the finished surface for the following machining of the posterior surface. During the re-blocking process on a blocking machine working in manual mode, the lens decentration errors and rotation errors which are inevitable and non-negligible will cause misalignment between the two surfaces.

The surface misalignment effect can be easily simulated by rotation and translation operation of the power vector matrices of lens surfaces. Here, the reference coordinate system is based on the posterior lens surface. Three types of misalignment, which are lateral misalignment, vertical misalignment and azimuthal misalignment, are introduced to the power vector matrix of anterior lens surface. In reality, the lateral and vertical alignment error within the range of ±1 mm can be expected and is mainly caused by the decentration of semi-finished lens blank. The in-plane rotation of the semi-finished lens blank normally leads to the azimuthal alignment error in the range of ±1 degree.

The simulation results shown in Fig. 8 demonstrate that the power distributions of DSOC-PAL design are insensitive to the lateral alignment error within at least ± 6 mm. This lateral alignment tolerance is attribute to the uniform surface power distribution along the horizontal direction of

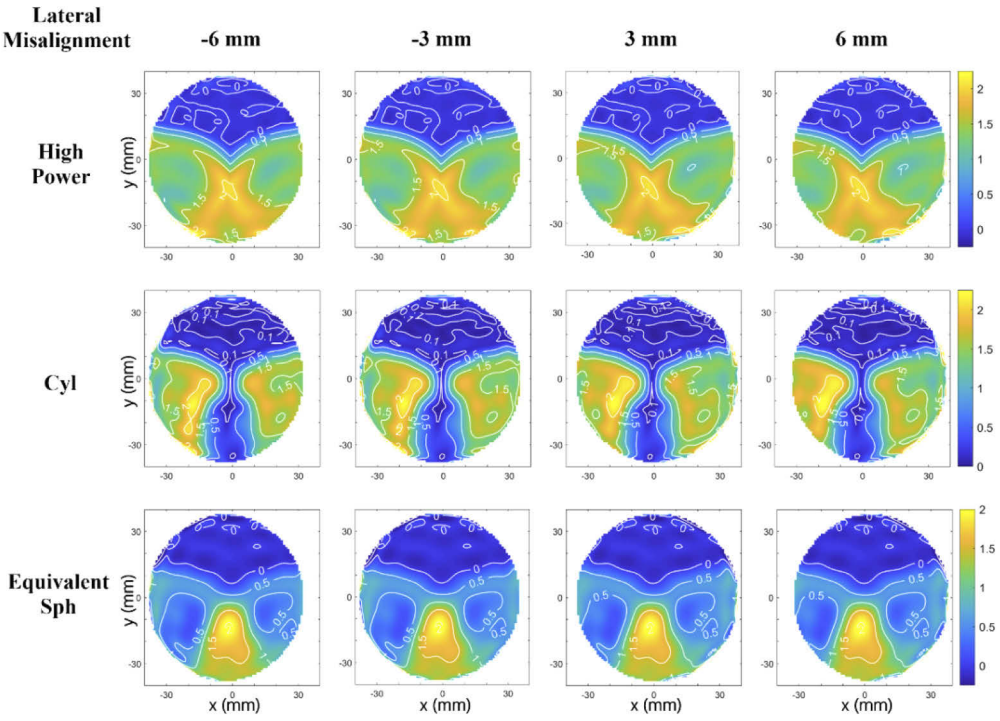

Fig. 8. The simulated lens power distribution influenced by lateral misalignment of −6 mm, −3 mm, 3 mm and 6 mm between the lens surfaces.

OSA CONTINUUM

anterior lens surface. This feature facilitates the intentional lens decentration designs aiming to match the pupil distance between two eyes.

The alignment tolerance in vertical direction is smaller than that of horizontal direction. As shown in Fig. 9, the vertical alignment error that exceeds the range of ± 2 mm will lead to a significant increase in the unwanted cylindrical power which can narrow down the progressive corridor. In practice, this vertical alignment error is not the main concern, because an engraving mark indicating the horizontal centerline on the finished anterior surface can help to align the semi-finished lens blank with the reference system of blocking machine.

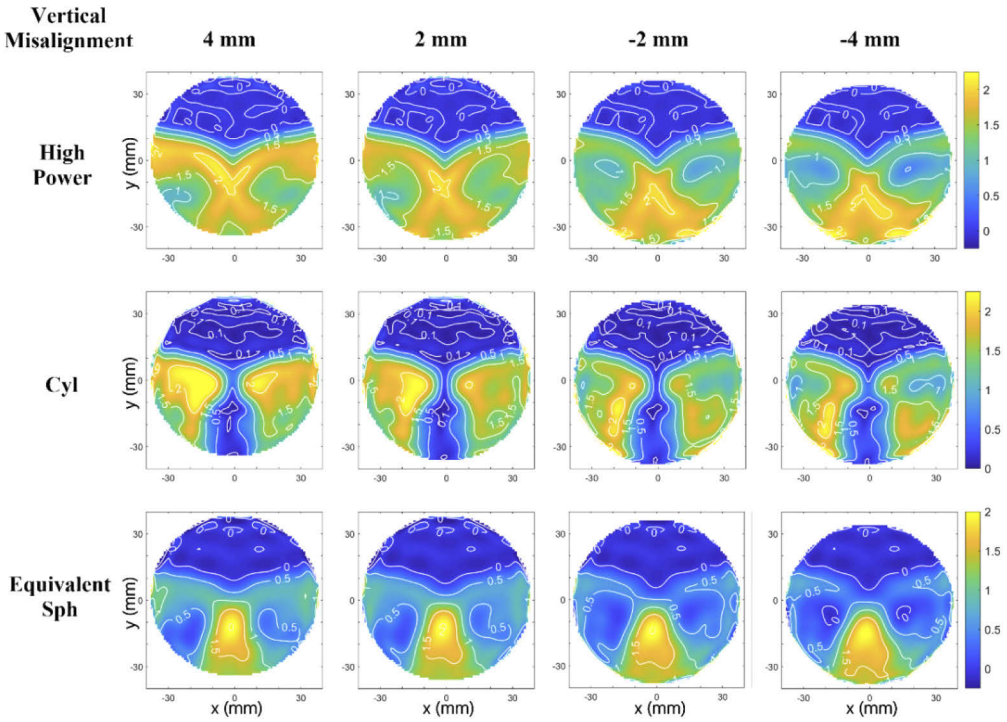

Fig. 9. The simulated lens power distribution influenced by vertical misalignment of −4 mm, −2 mm, 2 mm and 4 mm between the lens surfaces.

A great tolerance of at least ± 5° is allowed for the azimuthal misalignment in simulation as shown in Fig. 10. Within this tolerance, the azimuthal alignment error has little influence on the clear visual zone with unwanted cylindrical power of less than 0.5 diopter. Note that, besides lens blocking process, the mechanical error of positioning pole in the pneumatic chuck that can hold the lens blank firmly may be another source of azimuthal misalignment during the fixture of semi-finished lens blank on the aerostatic spindle. In general, a typical azimuthal misalignment within ± 2°, which is totally covered by our design tolerance, can be expected for DSOC-PAL manufacture with commercial lens production lines.

OSA CONTINUUM

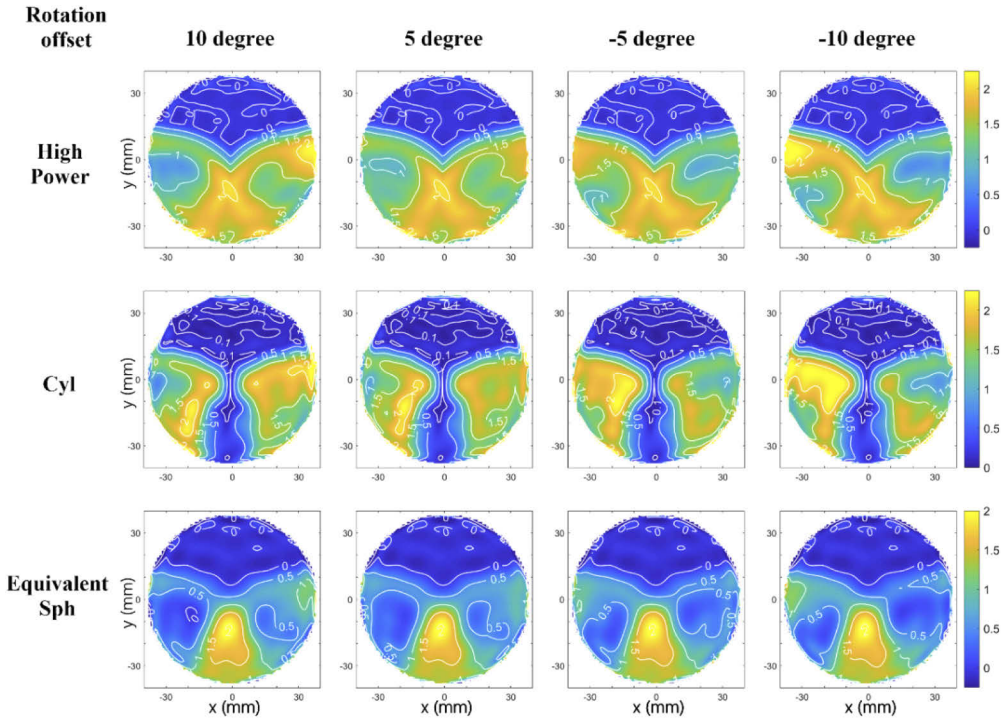

Fig. 10. The simulated lens power distribution influenced by azimuthal misalignment of −10°, −5°, 5° and 10° between the lens surfaces.

4. Experimental results

4.1. Tool path generation

In the case of progressive lens surfacing with a commercial freeform machining equipment, the designed lens surface should be rendered as a points file in standard format suggested by the Vision Council [23]. This file can be transmitted to the computer controller of the freeform generator, which will mathematically model the lens surface by using fitting method to calculate the tool path. The major drawback is the possible approximation error due to the limited accuracy in surface modelling. In our case, however, the standard points file is not necessary any more, as the lens surfacing is performed with a self-developed computer-numerically controlled (CNC) freeform generators [24]. We have developed a proprietary software using Matlab Programming to directly transfer the three-dimensional surface data with the high frequency freeform features into an appropriate format of CNC data for machining which can be free from surface modelling error.

The lens surface is well described with 0.52×10^6 supporting points in a polar mesh within an aperture of 78 mm in diameter. The point elements are equally spaced with an incremental size of 25 μm along radial direction. A circumferential spacing of 0.4 mm is used for points on the outer diameter, so the angular spacing will increase as the point approaches the lens center. As long as the angular spacing becomes larger than a threshold of 2°, a fixed angular increment instead of the fixed circumferential spacing is used to rule the remaining supporting points. The surface profile at all the points is calculated by using Zernike polynomials with the coefficients already shown in Fig. 3. The computation time of tool path for each surface is 2 minutes based on a desktop computer equipped with an Intel i7 processor of 1.8 GHz clock frequency.

OSA CONTINUUM

The lens surfacing process comprises rough cutting and finishing starting at the right edge and the left edge of the lens, respectively. Therefore, two different tool paths both following spiral trajectory are required for each surface as shown in Fig. 11. The anterior lens surface should be processed to be convex form which is the inverse version of the surface profile shown in Fig. 1(e). Here, the tool radius compensation is out of consideration. The reason is that the radius curvature of lens surface is much larger than the cutting edge radius of tool tip which is normally 2 mm. The tool radius correction in the radial direction can hardly have significant influence on the lens power measured in diopters, therefore can be neglected.

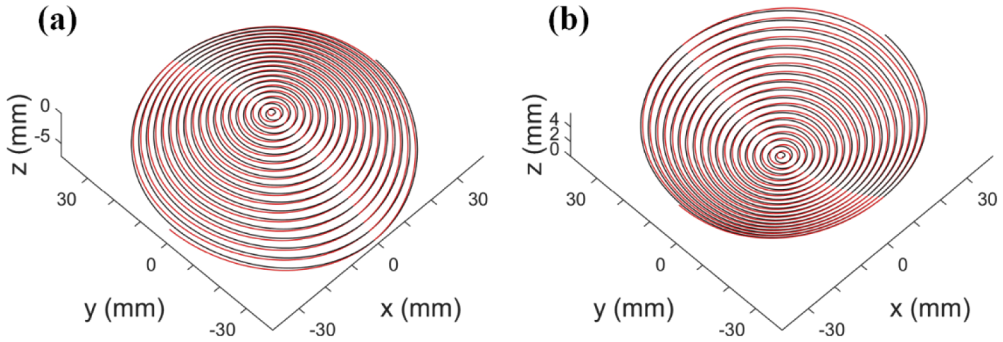

Fig. 11. The calculated tool path for (a) the convex anterior lens surface and (b) the concave posterior lens surface. The feed rate was set to be 2 mm per revolution just for demonstration. Black line: tool path for rough cutting; red line: tool path for finishing.

4.2. Lens surfacing and power measurement

To fabricate the DSOC-PAL, the surfaces of lens blank made of CR39 is subjected to a two-stage cutting process by freeform generator which uses a polycrystalline diamond tool for rough cutting with a depth of 0.5 mm and a natural diamond tool for a high-quality finishing with a cutting depth of 0.1 mm. This two-tool configuration is mounted on an FTS unit.

The total FTS stroke required is 2.2 mm and 0.9 mm for the machining of anterior surface and posterior surface, respectively. Limited by the working bandwidth and the tracking error of tool motion, the FTS is operated at 33.3 Hz with a constant spindle speed of 1000 rpm. The feed rate is 25 mm/min. After generating, the lens surfaces undergo a uniform polishing process with a flexible freeform polisher that uses a dynamically-controlled soft lap tool to remove the tool marks.

For comparison with the designed power distribution of each lens surface, we first fabricated only one surface of DSOC-PAL on a lens blank leaving the other spherical surface of lens blank unchanged. Then, a lens inspection system (Rotlex, Class Plus) operating on the Moire interferometer was used to measure the power profiles of the semi-finished lens blanks within an aperture of 60 mm in diameter as shown in Fig. 12. It should be noted that the constant spherical power of the untouched surface of lens blank has been subtracted from the measured high power distributions. The slight difference observed between Fig. 4 and Fig. 12 is mainly caused by the inertia of FTS and the inconsistent cutting conditions over the aperture of lens.

Finally, the semi-finished lens blank, whose anterior surface has been finished, undergoes a re-blocking process followed by a diamond turning and polishing on the posterior surface to give the DSOC-PAL. The re-blocking process has minor influence on the lens power distribution due to the considerable alignment tolerance between the two surfaces as discussed in Section 3. Figure 13 shows the measured power profiles of DSOC-PAL. The very good agreement with the designed power distribution supports our lens design model.

OSA CONTINUUM

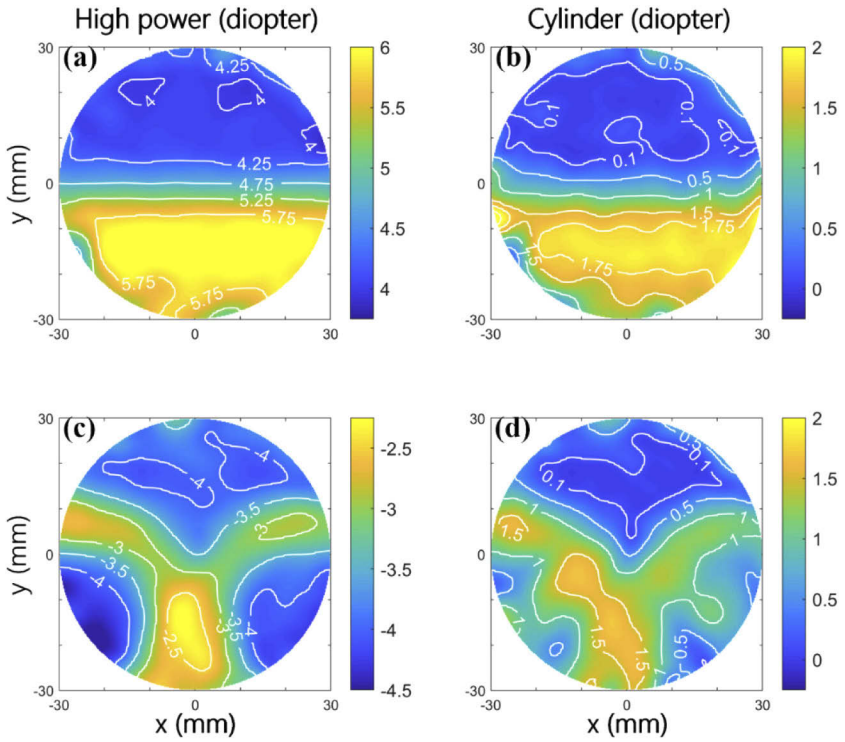

Fig. 12. The measured power distribution of the semi-finished lens blank. (a)~(b) Only the anterior surface of lens blank is finished; (c)~(d) Only the posterior surface of lens blank is finished.

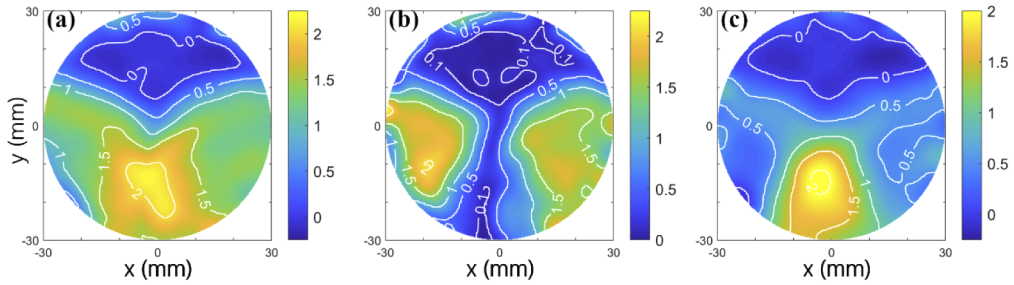

Fig. 13. The sphero-cylinder representation of the measured DSOC-PAL power in diopters including (a) high power, (b) cylindrical power and (c) equivalent spherical power.

5. Conclusion

We presented an efficient solution for the freeform surface design of DSOC-PAL. The new surface model is based on the minimization of a merit function which determines the power profiles across lens surface. The carefully constructed weight functions and boundary conditions result in accurate distributions of both the spherical power and the necessary cylindrical power with specified axial orientations. The proposed simple representation of power vector matrix delivers the lens power profiles based on the simulated surface powers.

We analyzed the surface misalignment of our lens model. Comparing the results to that of the perfect alignment situation in simulations implied that the design of our new DSOC-PAL is

OSA CONTINUUM

highly tolerant to alignment error. Finally, as an application example, we used the CNC multi-axis surfacing and polishing systems to produce these complex lens surfaces. The measured results verified the effectiveness of the proposed lens design method. As part of future investigation, the customized real-time design and production of individualized DSOC-PAL will be the most meaningful benefit to patients and lens industry.

Funding

National Natural Science Foundation of China (61775171); National Key Research and Development Program of China (2016YFC0100200).

Acknowledgments

The authors wish to thank Jisheng Xia and Risheng Xia for supplying the data communication standard of lens processing and also the valuable discussion about lens blocking process.

Disclosures

The authors declare no conflicts of interest.

References

1. J. E. Sheedy, "Progressive addition lenses-matching the specific lens to patient needs," Optometry **75**(2), 83–102 (2004).
2. A. Kitani and Y. Kikuchi, "Bi-aspherical type progressive-power lens," U.S. patent 6,935,744 (2005).
3. A. Kitani and Y. Kikuchi, "Bi-aspherical type progressive-power lens," U.S. patent 7,241,010 (2007).
4. B. Maitenaz, "Ophthalmic lenses with a progressively varying focal power," U.S. patent 3,687,528 (1972).
5. J. T. Winthrop, "Progressive addition spectacle lens," U.S. patent 4,861,153 (1989).
6. J. T. Winthrop, "Progressive addition spectacle lens," U.S. patent 5,123,725 (1992).
7. J. Loos, G. Greiner, and H. P. Seidel, "A variational approach to progressive lens design," Comput. Aided. Des. **30**(8), 595–602 (1998).
8. J. Wang, R. Gulliver, and F. Santosa, "Analysis of a variational approach to progressive lens design," SIAM J. Appl. Math. **64**(1), 277–296 (2003).
9. J. Wang and F. Santosa, "A numerical method for progressive lens design," Math. Models Methods Appl. Sci. **14**(04), 619–640 (2004).
10. W. Jiang, W. Z. Bao, Q. L. Tang, H. Q. Wang, and L. Zhu, "A variational-difference numerical method for designing progressive-addition lenses," Comput. Aided. Des. **48**, 17–27 (2014).
11. Y. Li, W. Huang, H. Feng, and J. Chen, "Customized design and efficient machining of astigmatism-minimized progressive addition lens," Chin. Opt. Lett. **16**(11), 113302 (2018).
12. V. Lakshminarayanan and A. Fleck, "Zernike polynomials: a guide," J. Mod. Opt. **58**(7), 545–561 (2011).
13. J. Liang, B. Grimm, S. Goelz, and J. F. Bille, "Objective measurement of wave aberrations of the human eye with the use of a Hartmann–Shack wave-front sensor," J. Opt. Soc. Am. A **11**(7), 1949–1957 (1994).
14. ISO, "Ophthalmic optics and instruments - Reporting aberrations of the human eye," in ISO 24157: 2008.
15. D. R. Iskander, M. J. Collins, and B. Davis, "Optimal modeling of corneal surfaces with Zernike polynomials," IEEE Trans. Biomed. Eng. **48**(1), 87–95 (2001).
16. R. R. Krueger, R. A. Applegate, and S. M. MacRae, "Wavefront Customized Visual Correction: The Quest for Super Vision II," Slack Incorporated, 2nd Edition (2003).
17. Y. Li, R. Xia, J. Chen, H. Feng, Y. Yuan, D. Zhu, and C. Li, "Freeform surface of progressive addition lens represented by Zernike polynomials," Proc. SPIE **9683**, 96830W (2016).
18. D. R. Ibañez, J. A. Gómez-Pedrero, J. Alonso, and J. A. Quiroga, "Robust fitting of Zernike polynomials to noisy point clouds defined over connected domains of arbitrary shape," Opt. Express **24**(6), 5918–5933 (2016).
19. A. Gray, E. Abbena, and S. Salamon, "Modern Differential Geometry of Curves and Surfaces with Mathematica," CRC Press (2006).
20. L. N. Thibos, W. Wheeler, and D. Horner, "Power vectors: an application of fourier analysis to the description and statistical analysis of refractive error," Optom. Vis. Sci. **74**(6), 367–375 (1997).
21. G. Minkwitz, "On the surface astigmatism of a fixed symmetrical aspheric surface," Opt. Acta **10**(3), 223–227 (1963).
22. J. Sheedy, M. Buri, I. Bailey, J. Azus, and I. Borish, "The optics of progressive lenses," Optom. Vis. Sci. **64**(2), 90–99 (1987).
23. Lens Processing & Technology Division of Vision Council, "Data communication standard," version 3.12 (2018).
24. H. Feng, R. Xia, Y. Li, J. Chen, Y. Yuan, D. Zhu, S. Chen, and H. Chen, "Fabrication of freeform progressive addition lenses using a self-developed long stroke fast tool servo," Int. J Adv. Manuf. Technol. **91**(9-12), 3799–3806 (2017).